

Robust Solid Electrolyte Interphase Induced by Dication Deep Eutectic Electrolytes for Sustainable Zn Anodes

Chunpeng Li, Jun Zhang, Kai Zhang, Anping Zhang, Wei Jian,* Ping Jiang,* Zhong-Shuai Wu, and Dianbo Ruan



Cite This: *ACS Sustainable Chem. Eng.* 2023, 11, 15470–15479



Read Online

ACCESS |

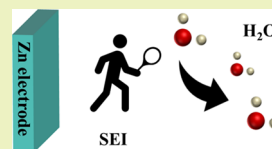
Metrics & More

Article Recommendations

Supporting Information

ABSTRACT: Aqueous Na–Zn ion batteries are promising for large-scale energy storage due to their low cost and high output voltage potential. However, the formed dendrites and notorious side reactions of zinc anodes lead to rapid performance degradation. Here, a sodium–zinc dication hybrid hydrated deep eutectic electrolyte system (NZDES) is proposed, in which organic ligands and all water molecules participate in NZDES's internal solvation structure networks, resulting in the suppressed side reaction at the Zn anode. Furthermore, the unique aqueous Zn^{2+} solvation shell is efficiently regulated by Na^+ , enabling high Zn deposition/stripping reversibility (96.5% Coulombic efficiency). Meanwhile, the decomposition of solvated methylsulfonylmethane (MSM) forms the enhanced solid electrolyte interphase, which improves the smoothness of the Zn anode and further suppresses the decomposition of water. With these merits, the CuHCF/Zn hybrid batteries with dication deep eutectic electrolytes exhibit a high capacity retention of >91.6% after 3000 cycles at 10 C with a 1.9 V open circuit voltage. The results provide a potential design strategy for an effective solid electrolyte interface for aqueous zinc ion batteries.

KEYWORDS: aqueous Na–Zn ion hybrid battery, hybrid hydrated deep eutectic electrolytes, solid electrolyte interphase, solvation structure, Zn anode



INTRODUCTION

Lithium-ion battery is the most successful rechargeable battery system for vehicle electrification and portable energy storage so far but suffer toxic organic electrolytes and inherent safety concerns.^{1,2} Rechargeable aqueous batteries are regarded as one of the most promising devices for grid-scale energy storage because of their low cost, eco-friendliness, high safety, and so forth.³ Among them, the aqueous Zn-ion batteries (AZIBs) have been considered as the potential candidates to be next-generation metal ion batteries due to their low standard reduction potential (-0.76 V vs SHE), high theoretical capacity (≈ 820 mA h g^{-1}), and perfect water compatibility of Zn metal anodes.^{4–6} For instance, significant progress of high discharge capacity above 200 mA h g^{-1} and ideal stability were obtained by $NH_4V_4O_{10}/Zn$,⁷ V_2O_5/Zn ,⁸ and MnO_2/Zn ,⁹ AZIBs. However, the sluggish diffusion of Zn^{2+} in the host material and the low discharge voltage (<1.8 V) limit the further development of AZIBs.⁴ Recently, the aqueous Na–Zn hybrid battery was proposed to circumvent the dilemma encountered by zinc-ion batteries based on the mechanism of Zn^{2+} ion deposition on the anode and Na^+ ion intercalation in the cathode.^{10–13} Prussian blue analogues (PBAs) with a stable three-dimensional framework for fast ionic diffusion have shown superiority as cathode materials with high Na^+ ion intercalation potential, and the Na–Zn hybrid battery has achieved a high open circuit voltage (OCV) of 2.0 V with Na^+ in the PBA cathode against the Zn anode.^{11,14} However, the main obstacle that needs to be overcome lies in the poor reversibility of the Zn anode in aqueous chemistry,^{15–18} which

is associated with the hydrated coordination environment of Zn^{2+} . The uneven deposition of zinc during the charging process with the participation of free water molecules causes severe chemical corrosion, H_2 evolution, and other side reactions, which lead to serious degradation of the electrochemical performance of zinc-based aqueous batteries.^{19–21} Therefore, many key strategies have been proposed to inhibit the formation of zinc dendrites and prevent the penetration of water to the zinc surface,^{8,21–26} such as adding electrolyte additives,^{9,22,27} modifying the anode interface,^{16,26,28} and raising the solute concentration.^{7,23} The key to effective electrolyte regulation is to weaken the bonding strength between Zn^{2+} ion and solvated H_2O , as well as in situ construct the uniform conductive solid electrolyte interphase (SEI) on the Zn anode.^{7–9,24–27,29,30} Deep eutectic solvent (DES) is considered as an emerging class of green electrolyte, with the superior properties of high thermal/chemical stability, low volatility and vapor pressures, nontoxicity, and low cost, which has received increasing attention in recent years.^{31–33} In addition, due to the interaction of complex anions and cations, DESs also have characteristics that other electrolytes do not possess, including nonflammability, ease of synthesis, structural

Received: August 3, 2023

Revised: September 26, 2023

Published: October 9, 2023



flexibility, and multielectron reactions.³² The original DES is generally obtained by simply mixing Lewis or Brønsted acids and bases in the eutectic molar ratio,³⁴ and the intensive interaction (hydrogen bond and coordinate bond) that existed in the DES between ions and solvate molecules make them strong for water solubility and moisture absorption. Introducing an appropriate amount of water can significantly affect the viscosity and conductivity properties of DES,^{34–36} and the coordination of Lewis acidic cations with oxygen donors in water or Lewis basic anions forms the cation-water–anion coordination complexes in the DES electrolyte. However, the hydration of coordination complexes has an upper limit, below which almost all water molecules participate in the solvation sheath, resulting in the suppressed activity of free water while the nature of DES is retained.^{34,37} For example, Tao and co-workers³⁸ proposed a good-performance eutectic electrolyte consisting of ZnCl₂, tetramethyl urea (TMU), and water, in which H₂O double-bonded with Zn²⁺ and TMU by coordination and hydrogen bonding, respectively, resulting in the greatly inhibited activity of H₂O and the highly reversibility process of Zn²⁺ plating/stripping. Methylsulfonylmethane (MSM) employed as the strong Lewis base in DES can form the cation (Li⁺ or Zn²⁺)-MSM-H₂O-anion solvation structure, leading effectively to the suppression of anode side reactions and promotion of the stability of aqueous lithium or ZIB.^{7,36} The DES based on succinonitrile (SN), urea, and acetamide are also investigated for the effect of cation solvent sheath structure on cycle reversibility.^{7,35,36,39} This favorable trend can be used to explore new aqueous electrolyte systems with customized adaptability to the Na–Zn hybrid battery.

Regarding the base in the DES solvent, the notably dielectric constant (47.39), dipole moment (4.44 D), and the abundant sulfonyl group of MSM make it a unique Lewis base candidate to coordinate with cations.^{7,32,36} Herein, we present a new type of low-cost MSM-based DES of dication electrolyte containing Na⁺ and Zn²⁺, which endows the Zn anode to exhibit unusual reversibility and durability. By adjusting the ratio of Na-DES and Zn-DES, the aqueous Na–Zn hybrid battery based on the CuHCF cathode and Zn anode possessing high energy density and long cycle is obtained. Combining the spectroscopic analysis and theoretical modeling, the water and MSM interactions of hybrid DES (NZDES) are revealed, and the water reactivity has been significantly suppressed while the ionic conductivity and viscosity are intensified. The Lewis basic MSM essentially participates in the primary solvation shell of Zn²⁺ or Na⁺ ion, and by introducing cation–O interactions between Zn²⁺/Na⁺ and MSM, the original [Zn(OH₂)₆]²⁺ species and [Na(OH₂)₆]⁺ convert to the Zn²⁺/Na⁺-(MSM)-(H₂O) solvation structure, which allows dendrite-free Zn plating/stripping with a high Coulombic efficiency (CE) of 96.5% in Cu||Zn battery. In addition, the effective SEI formed on the Zn anode restrains the side reaction between H₂O molecules and Zn anode, resulting in a pretty much stable cycle of 3200 h at the current density of 4 mA cm⁻¹ in Zn||Zn symmetric batteries. The hybrid Na–Zn battery with NZDES-2 delivers a high specific capacity of 72.6 mA h g⁻¹ at 1 C and 61.9 mA h g⁻¹ at 5 C together with an OCV of 1.9 V. In addition, the hybrid battery also achieves cycling stability over 3000 cycles at the current density of 10 C with 91.6% capacity retention. This work offers a promising electrolyte regulation strategy for the high performance of aqueous hybrid Na–Zn batteries.

EXPERIMENTAL SECTION

Synthesis of Cathode Materials. Copper hexacyanoferrate (CuHCF) was synthesized by a coprecipitation method. Typically, 100 mL of 0.05 M K₃Fe(CN)₆ (Aladdin) were added into an equal amount of 0.1 M Cu(NO₃)₂ (Sinopharm Chemical Reagent) solutions at the drop rate of 0.35 mL min⁻¹ under vigorous stirring conditions at room temperature. The yellow CuHCF precipitate was obtained after the reaction was completed. Then, CuHCF was then cleaned in deionized water and finally dried at 80 °C overnight.

Electrolyte Preparation. The Zn-DES electrolyte was prepared by dissolving Zn(ClO₄)₂·6H₂O (Aladdin) and MSM (Aladdin) by the molar ratio of 1:3. Also, the molar ratio of NaClO₄·H₂O (Aladdin), MSM, and H₂O in the Na-DES electrolyte is 1:1.5:1. The NZDES is obtained by mixing Na-DES and Zn-DES at the ratio of 25:1. Then, an appropriate amount of water was added to the NZDES electrolyte to obtain solutions with different molar ratios of [H₂O]/[Na⁺] (2, 4, 6, and 10, respectively), which are abbreviated as NZDES-2, NZDES-4, NZDES-6 and NZDES-10. Also, the mixed electrolyte of saturated NaClO₄ solution and saturated Zn(ClO₄)₂ solution at the same ratio of 25:1 without adding MSM was also prepared for comparison, named Sat-NZ.

Characterization. The morphology of CuHCF powder and Zn anode samples was analyzed by a Hitachi S-4800 field emission scanning electron microscope. Powder X-ray diffraction (XRD) patterns were collected by using an AXS D8 Advance diffractometer (Cu Kα radiation; receiving slit, 0.2 mm; scintillation counter, 40 mA; 40 kV) from Bruker Inc. Raman spectra were collected with a Renishaw in Via Reflex confocal microscopy Raman spectrometer and combined with a Fourier transform infrared spectrometer (FTIR, iSS0R, America) which were applied to characterize the coordination of electrolytes. X-ray photoelectron spectra (XPS) were recorded by using a Kratos AXIS Ultra XPS spectrometer.

Electrochemical Measurements. Electrochemical measurements were carried out on a LANHE Battery Tester and Solartron 1470E multichannel potentiostats. The depth of discharge (DOD) and stripping/plating tests of Zn were performed in Zn||Cu asymmetric cells and Zn||Zn symmetrical cells, respectively. The cathodes were prepared by mixing the corresponding CuHCF powder (80 wt %), Super P (10 wt %), and poly(vinylidene fluoride) (10 wt %) in *N*-methyl-2-pyrrolidinone. The CuHCF cathode mass loadings on the Ti mesh were about 5–10 mg. The CuHCF, Ag/AgCl electrode, and Pt gauze were employed as the working electrode, reference electrode, and counter electrodes, respectively. To validate the mixed hydrate eutectic electrolyte, the CuHCF||NZDES-2||Zn hybrid batteries were constructed for the electrochemical performance tests. Electrochemical impedance spectroscopy (EIS) and cyclic voltammetry (CV) measurements were conducted on Solartron 1470E multichannel potentiostats. The galvanostatic charge/discharge tests were recorded using a LANHE Battery Tester at 25 °C in 0.8–2.0 V for CuHCF||NZDES-2||Zn hybrid batteries in CR2032 coin cells. The current density of 1 C is 60 mA g⁻¹.

Molecular Dynamics Simulations. Molecular dynamics (MD) simulations are performed to study the solvation structure of Zn²⁺ and Na⁺ in the hybrid NZDES-2 electrolyte. The Zn(ClO₄)₂, NaClO₄, MSM, and H₂O are packed into the simulation box with the size of 7 × 7 × 7 nm³ and α = β = γ = 90° according to their mole ratio of 25:1:40.5:56. The Condensed-phased Optimized Molecular Potential for Atomistic Simulation Studies (COMPASS) force field is applied to describe the inter- and intramolecular interactions between molecules.⁴⁰ COMPASS has been parametrized and validated to investigate the material properties of condensed materials and electrolyte systems.^{7,41} The particle–particle–mesh (PPPM) solver is used to describe the long-range electrostatic interaction. The energy minimization based on the conjugate gradient algorithm is performed to obtain a stable structure. The system is equilibrated under the NPT ensemble at a constant temperature of 300 K and zero pressure for 500 ps to achieve an equilibrium state. The Andersen thermostat and Berendsen barostat algorithms are applied to control the temperature and pressure. All the simulations are performed in Materials Studio

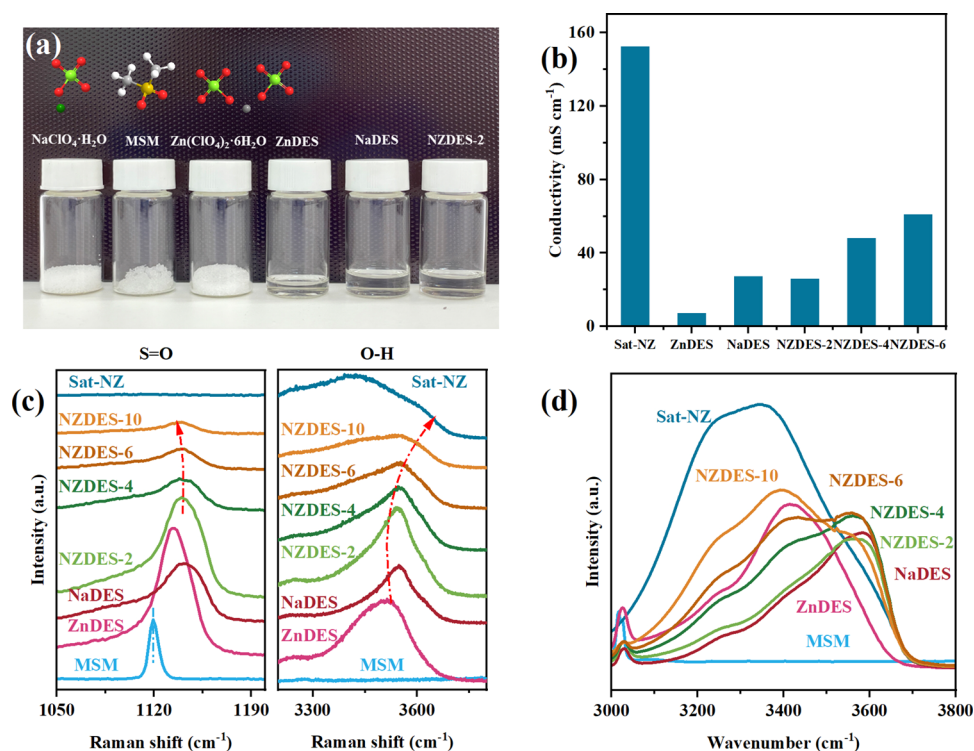


Figure 1. Preparation and physicochemical properties of the NZDES electrolyte. (a) Stoichiometric amounts of MSM, NaClO₄·3H₂O, and Zn(ClO₄)₂·6H₂O are used to prepare the NZDES. (b) Conductivity of the ZNDES-*n* solutions with increasing the water content (*n* = 2, 4, 6). (c) Raman and (d) FT-IR spectra of ZNDES-*n* electrolyte systems using the NaDES, ZnDES, and the saturated Sat-NZ (without MSM) as the references (*n* = 2, 4, 6, 10).

with an integration time step of 1 fs and periodic boundary conditions in all three dimensions. The radial distribution functions (RDFs), $g(r)$, that give the probability of atoms occurring at the distance r and the corresponding coordination number (CN) are calculated in order to analyze the ligand interaction with the solvent.

RESULTS AND DISCUSSION

Structure of Optimized NZDES. Due to the strong interaction between MSM and Na⁺/Zn²⁺, the formed Na⁺/Zn²⁺-MSM coordination serves as the strong Lewis acid in the DES, which can dissociate the crystal ionic salt by the “plasticizing” effect,⁴² resulting in the solubilization of Zn(ClO₄)₂ or NaClO₄. In this work, the ZDES composition of Zn(ClO₄)₂·6H₂O:MSM with the eutectic ratio of 1:3 shows the highest miscibility without additional water, and the eutectic ratio of NaClO₄·H₂O:MSM is 1:1.5 with adding a small amount of water (named NDES). The stable, transparent, colorless hybrid hydrated eutectic solvation (NZDES) was obtained by mixing NDES and ZDES at a certain ratio at room temperature (Figure 1a). Notably, the conductivity and viscosity of such hybrid hydrated eutectic system can be adjusted by adding a proportion of water, while retaining the original solvation structure when the added water is above the upper limit. Meanwhile, the endothermic peak decreases with increasing water content (Figure S1), which indicates that NZDES has a high proportion of water close to the aqueous solutions.

The electrochemical performance of the cathode is affected by the molar ratio of NDES:ZDES in hybrid NZDES electrolyte system, and the ratio of 25:1 in NZDES-2 with the conductivity of 26.0 mS cm⁻¹ shows the highest specific capacity and CE of 72.6 mA h g⁻¹ and 98.1%, respectively

(Figure S2). Since the physicochemical property of the hybrid NZDES electrolyte depends highly on its composition, structure, and dynamics, the intermolecular interactions among the solvent molecules of deep eutectic electrolytes were further studied for the fundamental understanding. The structural characteristics of NZDES were first explored by Raman, FTIR and DFT calculations (Figures 1c,d and S3–S7 in the Supporting Information). The O–H stretching vibration of mixed saturated aqueous electrolyte (Sat-NZ) shows a broad Raman band in the range of 3100–3700 cm⁻¹, which is similar to the strong hydrogen bonding in the water cluster.⁴³ With the decrease of the water content in NZDES, this peak diminishes and a new Raman band at 3550 cm⁻¹ starts to appear, indicating the process of hydrogen-bond breaking by MSM between water molecules and the water monomers in the solvation structure of Zn²⁺ or Na⁺.^{43,44} The 3550 cm⁻¹ cm peak and 3300 cm⁻¹ shoulder in the Raman spectra are assigned to the coordinate-water and free-water in NZDES, respectively. The weak shoulder band indicates that the proportion of free water is significantly reduced, and almost all water molecules participate in the Zn²⁺ or Na⁺ hydration shell. In addition, the Raman bands at 390 and 189 cm⁻¹ belong to the symmetric stretch of the octahedral [Zn(OH₂)₆]²⁺^{33,45} and [Na(OH₂)_{*n*}]⁺ (*n* = 4,5)⁴⁶ that disappear almost in NZDES-2 (Figure S3), respectively, suggesting that the structure of cation-water clusters is severely disturbed by the MSM molecular. Similar results are also obtained from FTIR spectra (Figures 1d and S5 in the Supporting Information). Two distinctive peaks at 3250 and 3350 cm⁻¹ can be observed in the Sat-NZ solution, which are assigned to the symmetric and asymmetric O–H stretching vibrations of the water cluster. Nonetheless, the intensities of the above two peaks decrease

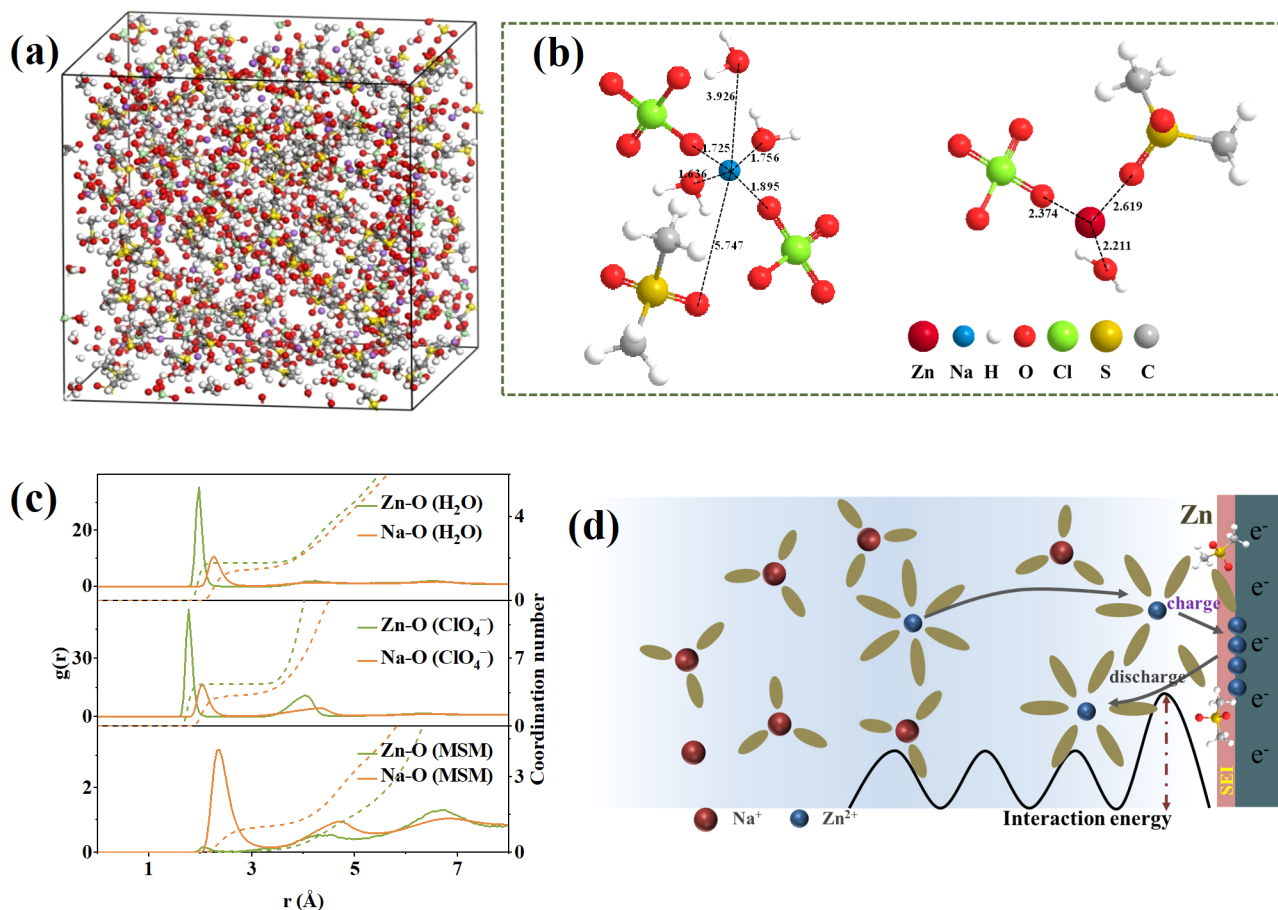


Figure 2. MD Simulations and the interface reactions of the Zn anode in the NZDES-2 electrolyte. (a) 3D snapshot obtained by MD simulations and (b) representative Na^+ and Zn^{2+} solvation structures in the NZDES-2 electrolyte. (c) RDFs for Na/Zn–O (H_2O), Na/Zn–O (ClO_4^-), and Na/Zn–O (MSM) of Na^+ and Zn^{2+} collected from MD simulations in the NZDES-2 electrolyte. (d) Schematic diagrams of the Zn^{2+} solvation structure and corresponding interfacial reactions in the NZDES-2 electrolyte.

gradually with the reduction of water content, while the intensity of the coordinate water broad peak shows an opposite trend at 3580 cm^{-1} . It indicates that the aggregated water through H-bonds nearly does not exist in NZDES-2, and they are isolated from each other by forming $\text{Na-H}_2\text{O}$ or $\text{Zn-H}_2\text{O}$ coordinate complex.^{7,33,39} Clearly, introducing MSM as the Lewis basic ligand may lead to a deviation of the solvation structure from that of a traditional aqueous solution. The Raman spectra of the S=O symmetric stretching (at 1140 cm^{-1} in NZDES-2) have been reported to be sensitive to the coordination of cations.⁴⁷ As shown in Figure 1c, the shift of the S=O peak in NaDES is larger than that in ZnDES, implying that the coordination of Na^+ -MSM is stronger than that of Zn^{2+} -MSM, and it becomes broadened accompanied by a redshift and the decreased intensity, suggesting that the excess water has hindered the coordination between Zn^{2+} or Na^+ and MSM. Additionally, the bands at ~ 1130 and $\sim 930\text{ cm}^{-1}$ correspond to the asymmetric and symmetric stretching vibration modes of the hydrated unperturbed ClO_4^- with the Td symmetry in Sat-NZ⁴³ (Figure S5), respectively. When the content of water is reduced in NZDES, the vibration of ClO_4^- shifts slightly accompanied by an increase in intensity, indicating that ClO_4^- interacts directly with cations and participates in the cation- H_2O -MSM shell. This indicates that the dissolved H_2O in NaDES is replaced by anions, resulting in the accumulation of H_2O at the interface being replaced by more electrochemically stable anions. In sum, Zn^{2+} or Na^+

cations are coordinated with MSM, H_2O , and ClO_4^- to form $\text{Zn}^{2+}/\text{Na}^+$ -coordinated complexes, in which MSM is double-bonded with cations and H_2O by coordination and hydrogen bonding.^{9,36}

Molecular dynamics (MD) simulations together with the resulting radial distribution functions (RDFs), which reveal the distribution of nearest-neighbor molecules at a certain distance, were performed to elucidate the solvation structures of Zn^{2+} and Na^+ from the nanoscale perspective. It is clear from Figure 2a that MSM, ClO_4^- , and H_2O -coordinate Zn^{2+} and Na^+ complexes exist in NZDES-2, which concur with the mass spectroscopy results in Figures 1c,d and S3–S5. The corresponding RDFs and coordination results also provide additional evidence of a Zn^{2+} and Na^+ (central ion) coordination environment (Figure 2b). The sharp peaks of the Zn–O pair and the Na–O pair correspond to the primary solvation shell of Zn^{2+} and Na^+ ions. Notably, the weak peaks of the Zn–O pair imply that the ClO_4^- anion and MSM molecule enter the second solvation shell. Combined with Raman data, it is clear that MSM molecules prefer to tightly coordinate to the solvation sphere of Na^+ than that of Zn^{2+} in NZDES, which is dramatically different from the coordinate state in Zn-DES.^{7,33} Further analysis of the RDFs of the Zn–O and Na–O pair demonstrates that the water molecules and ClO_4^- anions tend to surround Zn^{2+} . The average coordination number (CN) of Zn– H_2O in the first hydration shell is similar to that of Na– H_2O (CN = 1.7 and 1.4, respectively), while the

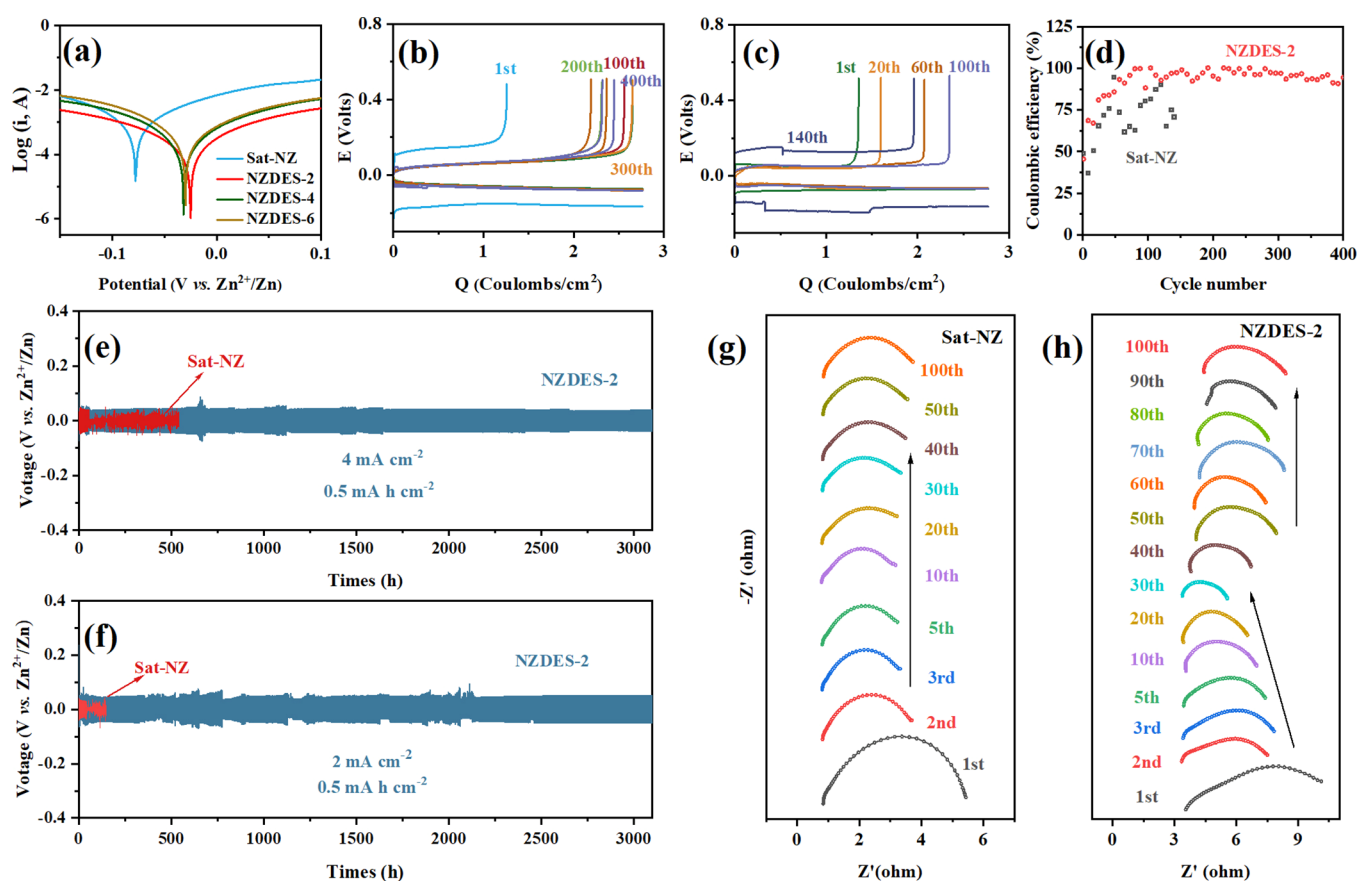


Figure 3. Electrochemical performance of the Zn anode in NZDES-2 and Sat-NZ electrolytes. (a) Linear polarization curves of zinc anodes in NZDES- n ($n = 2, 4, 6$) compared with Sat-NZ. (b, c) Galvanostat result of Cu||Zn plating/stripping curves and (d) CE in NZDES and Sat-NZ at a current density of 0.5 mA cm^{-2} and an area capacity of 0.5 mAh cm^{-2} (final voltage of 0.5 V). (e, f) Cycling stability of Zn||Zn symmetric batteries in NZDES and Sat-NZ electrolytes at 4 and 2 mA cm^{-2} . (g, h) Nyquist plots of the Zn||Zn symmetric batteries with NZDES-2 and Sat-NZ electrolytes in different cycles.

CN of Na-MSM (CN = 1.0) is larger than that of Zn-MSM. The modulated solvation structure of NZDES-2 with the reduced active water may be beneficial to the interfacial charge transfer and the uniform Zn plating.^{12,33,39,48} In addition, the interaction energy of Zn-MSM (-4.84 eV) in NZDES-2 is much weaker than Zn-H₂O (-30.16 eV), implying that MSM tends to easily dissociate than H₂O during the desolvation process of Zn²⁺ coordination complexes, and the H bond between MSM and H₂O molecule³⁶ will inhibit the ionization of H₂O during the desolvation process of Zn²⁺, which may be accounted for the inhibited hydrogen evolution and the effective SEI formation on the Zn anode.

Electrochemical Performance of the Zn Anode in the NZDES-2 Electrolyte. The corrosion behaviors of Zn anodes in Sat-NZ and NZDES- n ($n = 2, 4, 6$) were evaluated by linear polarization tests (Figure 3a). The lower corrosion current and more positive corrosion potential indicate higher electrochemical stability and corrosion resistance of NZDES-2 for Zn metal,⁴⁹ which can protect Zn anodes from serious hydrogen evolution corrosion during cycling compared with the aqueous system. Zn||Cu coin-type cells were employed to evaluate the CE of Zn plating/stripping at a practical deposition capacity of 0.5 mA h cm^{-2} and a current density of 0.5 mA cm^{-2} (Figure 3b,c). A high CE is significant for evaluating the cycle life of the metallic anode. The fluctuant voltage signals were both seen in cells based on the NZDES-2 and Sat-NZ electrolyte. The Zn||Cu half-cell in the NZDES-2 electrolyte shows a much

higher average CE of 96.5% compared to that of the Sat-NZ electrolyte ($\sim 75.8\%$). The CE of NZDES-2 improved over 100 cycles due to the formation of SEI (Figure 3b,d), resulting in a steady overpotential increase of $\sim 20 \text{ mV}$ (Figure S8). The stabilities of the Zn anode in both NZDES-2 and Sat-NZ electrolytes were evaluated at the current of 4 and 2 mA cm^{-2} with the capacity of 0.5 mA h cm^{-2} using symmetrical Zn||Zn cells. As illustrated in Figure 3e,f, the Zn||Zn cell operates sustainably over 3200 h in the NZDES-2 electrolyte without notable overpotential fluctuation, and the larger overpotential may be caused by the reduced ionic conductivity and the increased SEI resistance. In stark contrast, the unstable voltage response in Sat-NZ electrolytes was correspondingly maintained for only 500 and 100 h, respectively. At the same capacity, when the current decreases from 4 to 1 mA cm^{-2} , Zn||Zn cells show almost similar overpotential for Zn plating/stripping (Figures 3e,f, S9, and S10), which implies a high ionic conductivity of SEI formed on the Zn anode. The SEI formation process during Zn plating/stripping achieved by using the NZDES-2 electrolyte is further confirmed by comparison of impedance evolution, and the thickness of the formed SEI increases with cycling (Figure S11), which facilitates superior stability. The Zn||Zn cell assembled with the Sat-NZ electrolyte demonstrates a stable cell resistance during 100 cycles (Figure 3g). In contrast, the overall cell resistance of the symmetric cell with the NZDES-2 electrolyte continuously shifts to higher values followed by a regular

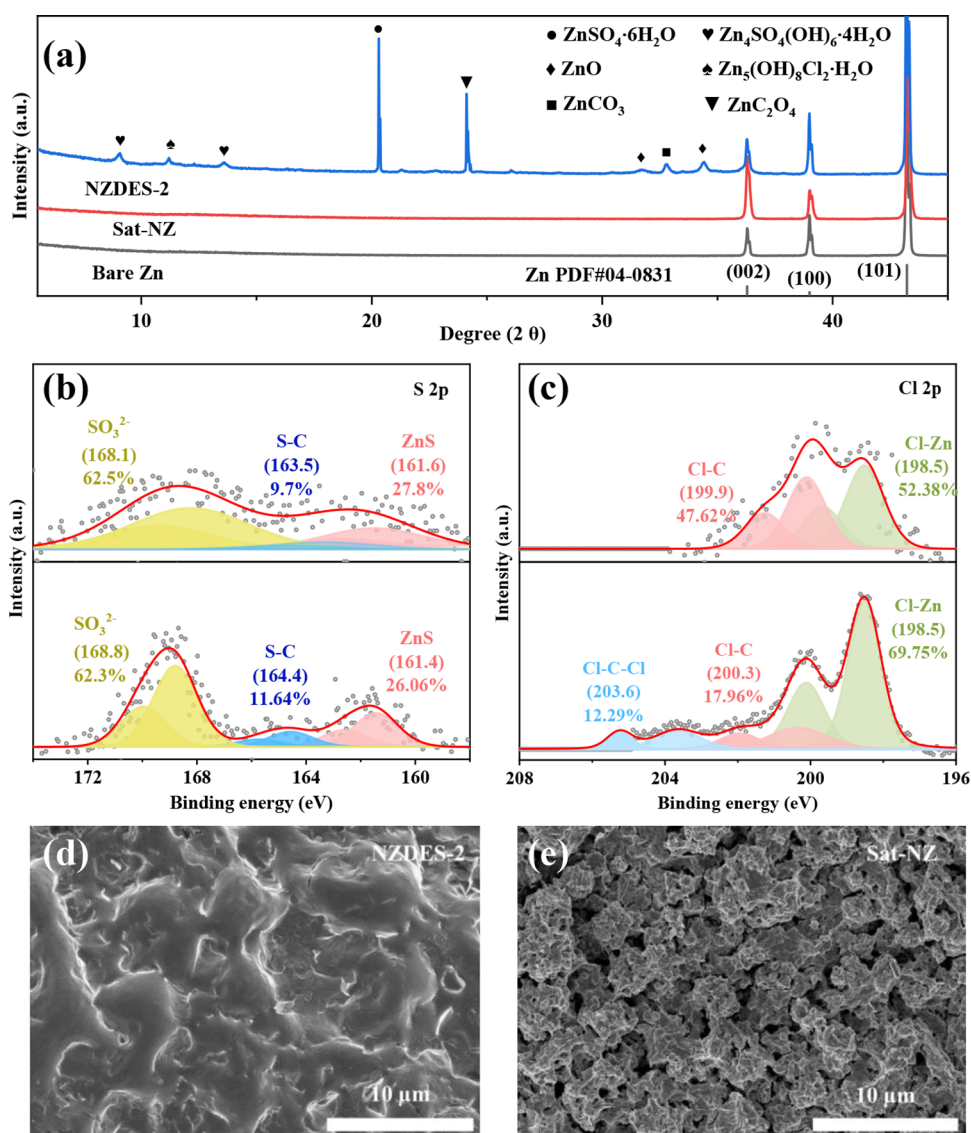


Figure 4. Characterization of SEI formed on the Zn anode. (a) XRD patterns of Zn anodes after plating/stripping cycles in NZDES-2 and Sat-NZ electrolytes. (b, c) XPS with Ar⁺ sputtering 0 min (top) and 30 min (bottom) of the SEI formed on Zn cycled in the NZDES-2 electrolyte. The S 2p and Cl 2p XPS spectra are displayed in columns. (d, e) SEM images of the Zn anode surface after 100 cycles in (d) NZDES-2 and (e) Sat-NZ electrolytes.

decrease of interfacial resistance from 2 to 30 cycles and irregular changes after 30 cycles (Figure 3h). This corroborates the implication that the formed SEI is unstable, and the deposition and dissolution of SEI occur continuously at the electrode/electrolyte interface until the dynamic equilibrium is reached. The gradual increase of CE before 80 cycles also confirms the formation process of SEI (Figure 3d), which can effectively prevent water from reacting with the Zn anode.

SEI on the Zn Anode. The SEI formed on the Zn anode derived from the reduction of the solvated MSM is analyzed by XRD and XPS characterizations. XRD (Figures 4a and S12) demonstrated that random zinco-phobic Zn₅(OH)₈Cl₂·H₂O byproducts were formed in the SEI, which can effectively suppress Zn dendrite growth.^{50,51} The smooth surface is shown in the optical image (Figure 4d). Additionally, the Zn²⁺-conductive composition in the SEI layer is formed in the NZDES-2 electrolyte as evidenced by the characteristic peaks of ZnC₂O₄ and ZnSO₄·6H₂O crystals. However, the XRD also exhibits Zn₄SO₄(OH)₆·4H₂O diffractions peak with low

density, which is formed by the HER process and causes local pH increase.^{7,8,25} By comparison, no SEI formed on the Zn anode in the Sat-NZ electrolyte, but the increased density of the (002) peak of Zn indicates the formation of a Zn dendrite. The detailed composition distribution in the top surface of SEI was also further analyzed by XPS (Figures 4b,c, S13, and S14). The S 2p spectrum shown in Figure 4b demonstrated that the formed outer layer of SEI in NZDES-2 electrolyte mainly contains inorganic ZnSO₃ (62.5%) and ZnS (27.8%) with few organic S–C species (9.7%). An insignificant increase in the organic S–C species and inorganic ZnS in the inner layer of SEI after 30 min of Ar⁺ sputtering is also observed. CO₃²⁻ signals detected from C 1s and O 1s spectra on the Zn electrode recovered from the NZDES-2 electrolyte (Figure S13), consistent with the previous report,⁹ which further confirmed the decomposition of MSM molecules. In addition, the Cl 2p spectrum of organic chlorine evolved from the reaction products between Zn(ClO₄)₂ and MSM, while the inorganic chlorine evolved from the precipitation of the

electrolyte. The inorganic Zn–Cl content increased from 52.4 to 69.8% at 30 min. What's more, the presence of organic Cl–C–Cl species in the inner layer of SEI could also contribute to high ionic conductivity, as it was absent on the Zn surface recovered from the NZDES-2 electrolyte or in the original salts. By contrast, no Cl–C–Cl species was found in Cl 2p spectroscopy of the Zn electrode recovered from the Sat-NZ electrolyte. It is expected that any species generated from MSM and ClO_4^- species decomposition may precipitate on the Zn anode surface, which allows Zn^{2+} to diffuse through the pores and provide kinetic protection against H_2 evolution by blocking water.

Electrochemical Performance of the Zn||CuHCF Na–Zn Hybrid Battery. The XRD pattern of obtained CuHCF (Figure 5a) agrees well with the cubic structure with a $Fm\bar{3}m$ space group (JCPDS 86–0513). The inset SEM image shows irregular CuHCF nanoparticles ranging in size from dozens to several hundred nanometers. The NZDES-2 electrolyte was evaluated in a coin cell using CuHCF as the cathode and Zn as the anode. The linear sweep voltammetry (LSV) technique was employed to evaluate the electrochemical window (EW) of NZDES-2 in a three-electrode cell with a Ti foil as the working electrode (Figures 5b and S15), and it exhibits the significantly expanded EWs of 2.92 V, which affords the valid Zn||CuHCF Na–Zn hybrid battery as the equilibrium potential of the CuHCF cathode and the Zn anode is at about 0.93 and -0.73 V, respectively. In Sat-NZ electrolytes, the hydrogen and oxygen evolution reactions (HER and OER) are clearly indicated by two irreversible processes: OER at 1.15 V and HER at about -0.35 V. Because the operation potentials of Zn are below the stability limits, the active materials unfortunately exhibit low CE and obvious capacity fading. The CV curves of the CuHCF cathode and the Zn anode in the NZDES-2 electrolyte are shown in Figure 5b, which demonstrate a reversible extraction/insertion process and electrochemical Zn plating/stripping, respectively. A pair of weak shoulder peaks (vs Zn/Zn^{2+}) at 0.55 V followed by a pair of strong redox peaks at 1.03 V, which is attributed to the preferential insertion of Na^+ into CuHCF rather than Zn^{2+} .¹³ Ex-situ XRD is used to analyze the structural evolutions of CuHCF at different charge and discharge states with electrochemical cycling. As shown in Figure 5c, the (111) peak near 43.5° of the steel current collector is used as a reference, and it shows no peak shift during cycling. The (200) and (220) peaks in XRD reflections are chosen as the representative peaks and show reversible shifts during the charging/discharging process in the NZDES-2 electrolyte, as well as a similar trend can be observed in other peaks. Besides, Na^+ -insertion into CuHCF leads to lattice contraction, which is consistent with the other literature.^{11,52} Obviously, the XRD patterns of CuHCF exhibit no observable change in the crystal structure upon cycling, indicating the highly reversible nature of the CuHCF crystal structure and the extended lifetime with Na^+ insertion/extraction. Since CuHCF and Zn perform the unique electrochemical behaviors in NZDES-2, Zn||CuHCF Na–Zn hybrid batteries are assembled. Its galvanostatic profiles at a rate of 1.2 C along with those of the individual Zn anode and CuHCF cathode are shown in Figure 5d. The average voltage output of the Na–Zn hybrid battery is about 1.55 and 1.46 V at 1 and 5 C, respectively (Figure S17), and the energy density of 112.53 Wh kg^{-1} based on the mass of cathode active materials is obtained. In addition, Zn||CuHCF based on the NZDES-2 electrolyte exhibits an excellent high-

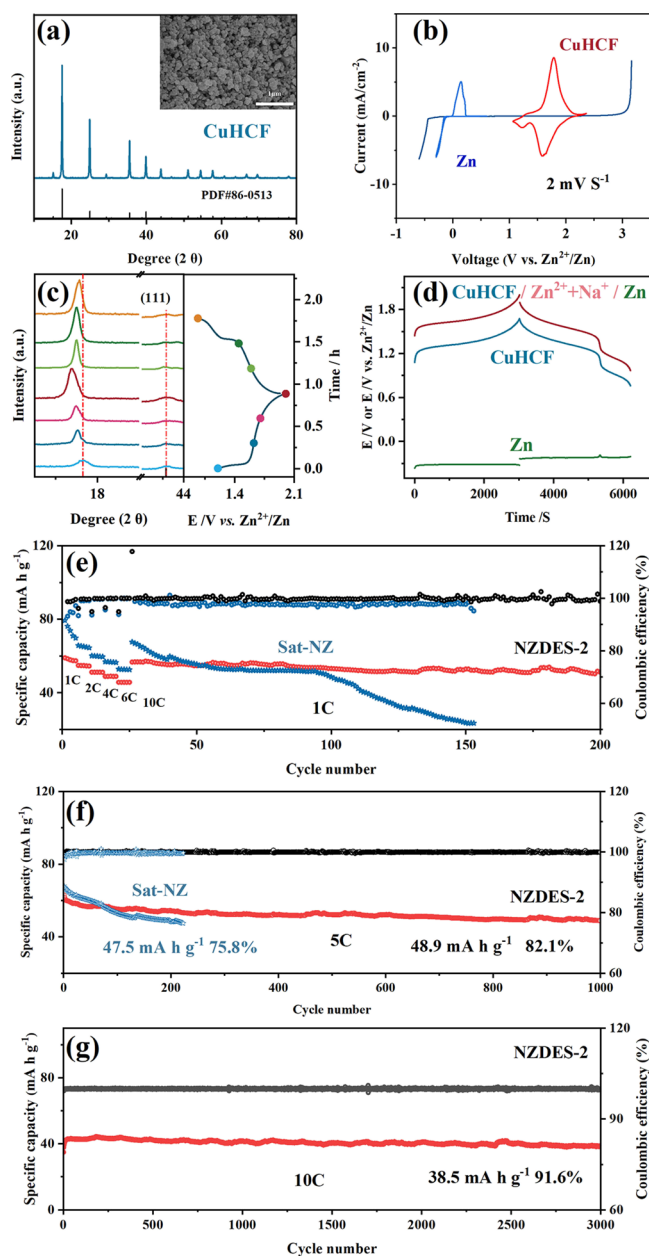


Figure 5. XRD of CuHCF and the electrochemical performance of Zn||CuHCF hybrid batteries. (a) XRD pattern of the obtained CuHCF materials. (b) LSV of current collector Ti and cyclic voltammograms (CVs) of CuHCF and Zn electrodes in the NZDES-2 electrolyte. (c) Ex situ XRD patterns of CuHCF with cycling. (d) Galvanostatic profiles of the Zn||NZDES-2||CuHCF battery along with the voltage profiles of their individual anode and cathode electrodes at a rate of 1.2 C. (e–g) Rate and cycling performance of Zn||CuHCF hybrid batteries in NZDES and Sat-NZ electrolytes at the rate of 1, 5, and 10 C.

rate capability as the capacity retains 71% retention at the rate of 10 C (Figure 5e). Its CE increases from 98.4% (1 C) to 99.9% (10 C) with an increasing charge rate, and about 86.5% retention of the initial discharge capacity is obtained after 200 cycles at 1 C. Under the rate of 2 and 4 C, as shown in Figure S17, the capacity decreases to 83.6 and 82.1% retention after 800 and 1000 cycles, respectively. Meanwhile, at a high rate of 5 C for 1000 cycling and 10 C for 3000 cycling, the capacity retention is 82.1 and 91.6%, respectively (Figures 5f and S18).

As a comparison, although the Zn||CuHCF based on the Sat-NZ electrolyte shows higher capacity than that based on the NZDES-2 electrolyte at the same rate conditions, the CE is lower and the capacity of Zn||CuHCF in the Sat-NZ electrolyte decays rapidly after 100 cycles. The rapid decay of capacity is also discovered at the rate of 2, 4, and 5 C (Figure S17). The capacity decay of Zn||CuHCF in the Sat-NZ electrolyte is mainly attributed to the low CE of Zn plating/stripping. The gradually decreasing impedance of the Zn||CuHCF cell based on the NZDES-2 electrolyte demonstrates the formation of effective SEI (Figure S19), which is beneficial for high CE and promotes stability. Thus, the high stability of the Zn||CuHCF in NZDES-2 electrolyte is superior to most state-of-the-art aqueous-based Na–Zn hybrid batteries (Table S1), indicating that the side reactions are highly suppressed during the cycling process despite the high voltage charging limit (2.1 V). Regarding the desolvation of the Zn^{2+} solvation structure, the discharging process generates more free-MSM and free-water molecules on the Zn anode surface. It is reasonably considered that the hydrogen bonding between MSM and water molecules can partially limit the rapid decomposition of water^{7,36} and benefit the formation of effective SEI on the Zn electrode/electrolyte interface,^{38,53,54} as well as the Na^+ can suppress the Zn dendrite deposition,⁴⁸ which are all beneficial to the stability of Na–Zn hybrid batteries.

CONCLUSIONS

We proposed a new type of mixed ion electrolyte based on low eutectic solvent for an aqueous Na–Zn hybrid battery system. In the NZDES-2 electrolyte, MSM replaces solvated H_2O in the $[\text{Zn}(\text{OH}_2)_6]^{2+}$ species, resulting in a decreased activity of water. Combined with the hydrogen bond of $\text{Zn}^{2+}\text{-H}_2\text{O}$, the decomposition of H_2O is highly suppressed. Meanwhile, this dual-coordination of $\text{Zn}^{2+}\text{-H}_2\text{O}\text{-MSM}$ results in the solvate MSM being preferentially reduced in situ to form the self-healing SEI on the Zn anode. The SEI allows Zn^{2+} transport but blocks H_2O immersion, which further inhibits the H_2 evolution and the growth of the Zn dendrite. Therefore, the Zn||CuHCF hybrid batteries fabricated in the NZDES-2 electrolyte show good stability of 91.6% after 3000 cycles at the rate of 10 C, and the CE of Zn plating/stripping is improved to nearly 99.8%. In addition, the Na–Zn hybrid battery delivered a high initial capacity of nearly 61.7 mA h g^{-1} and a high energy density of 90.1 Wh kg^{-1} at the high rate of 5 C. The low-cost NZDES electrolyte provides a full battery solution for high-performance hybrid power batteries, which has great significance for the practical application of Na–Zn hybrid batteries.

ASSOCIATED CONTENT

Supporting Information

The Supporting Information is available free of charge at <https://pubs.acs.org/doi/10.1021/acssuschemeng.3c04872>.

FT-IR and Raman spectra; interaction energy information; electrochemical comparison of NZDES-2 and Sat-NZ electrolytes; SEM and XPS spectra; XRD spectra of the Zn anode; cycling performance and EIS spectra of full cell in different electrolytes; and table of performance comparison of aqueous Zn batteries (PDF)

AUTHOR INFORMATION

Corresponding Authors

Ping Jiang – Institute of Advanced Energy Storage Technology and Equipment, Ningbo University, Ningbo 315201, China; orcid.org/0000-0001-9802-0955; Email: jianwei@nbu.edu.cn

Wei Jian – Institute of Advanced Energy Storage Technology and Equipment, Ningbo University, Ningbo 315201, China; Email: jiangping1@nbu.edu.cn

Authors

Chunpeng Li – Institute of Advanced Energy Storage Technology and Equipment, Ningbo University, Ningbo 315201, China

Jun Zhang – Advanced Li-Ion Battery Engineering Laboratory, Ningbo Institute of Materials Technology and Engineering, Chinese Academy of Science, Ningbo 315201, China

Kai Zhang – Key Laboratory of Advanced Energy Materials Chemistry (Ministry of Education), College of Chemistry, Nankai University, Tianjin 300071, China; orcid.org/0000-0001-8038-745X

Anping Zhang – State Key Laboratory of Catalysis, Dalian Institute of Chemical Physics, Chinese Academy of Sciences, 116023 Dalian, China

Zhong-Shuai Wu – State Key Laboratory of Catalysis, Dalian Institute of Chemical Physics, Chinese Academy of Sciences, 116023 Dalian, China; orcid.org/0000-0003-1851-4803

Dianbo Ruan – Institute of Advanced Energy Storage Technology and Equipment, Ningbo University, Ningbo 315201, China; orcid.org/0000-0001-8115-958X

Complete contact information is available at:

<https://pubs.acs.org/10.1021/acssuschemeng.3c04872>

Notes

The authors declare no competing financial interest.

ACKNOWLEDGMENTS

The authors acknowledge financial support from the Natural Science Foundation of Zhejiang Province (Grant No. LQ23B030007), Zhejiang Province Science and Technology Plan Project (Grant No. 2022C01072), and Ningbo Science and Technology Plan Project (Grant No. 2022Z021 and No. 2022Z026).

REFERENCES

- (1) Fan, X.; Wang, C. High-voltage liquid electrolytes for Li batteries: progress and perspectives. *Chem. Soc. Rev.* **2021**, *50* (18), 10486–10566.
- (2) Yang, L.; Yang, K.; Zheng, J.; Xu, K.; Amine, K.; Pan, F. Harnessing the surface structure to enable high-performance cathode materials for lithium-ion batteries. *Chem. Soc. Rev.* **2020**, *49* (14), 4667–4680.
- (3) Liu, J.; Xu, C.; Chen, Z.; Ni, S.; Shen, Z. X. Progress in aqueous rechargeable batteries. *Green Energy Environ.* **2018**, *3* (1), 20–41.
- (4) Konarov, A.; Voronina, N.; Jo, J. H.; Bakenov, Z.; Sun, Y.-K.; Myung, S.-T. Present and Future Perspective on Electrode Materials for Rechargeable Zinc-Ion Batteries. *ACS Energy Lett.* **2018**, *3* (10), 2620–2640.
- (5) Zhang, N.; Chen, X.; Yu, M.; Niu, Z.; Cheng, F.; Chen, J. Materials chemistry for rechargeable zinc-ion batteries. *Chem. Soc. Rev.* **2020**, *49* (13), 4203–4219.
- (6) Lin, D.; Li, Y. Recent Advances of Aqueous Rechargeable Zinc-Iodine Batteries: Challenges, Solutions, and Prospects. *Adv. Mater.* **2022**, *34* (23), No. 2108856.

- (7) Han, M.; Huang, J.; Xie, X.; Li, T. C.; Huang, J.; Liang, S.; Zhou, J.; Fan, H. J. Hydrated Eutectic Electrolyte with Ligand-Oriented Solvation Shell to Boost the Stability of Zinc Battery. *Adv. Funct. Mater.* **2022**, *32* (25), No. 2110957.
- (8) Cao, J.; Zhang, D.; Yue, Y.; Chanajaree, R.; Wang, S.; Han, J.; Zhang, X.; Qin, J.; Huang, Y. Regulating solvation structure to stabilize zinc anode by fastening the free water molecules with an inorganic colloidal electrolyte. *Nano Energy* **2022**, *93*, No. 106839.
- (9) Cao, L.; Li, D.; Hu, E.; Xu, J.; Deng, T.; Ma, L.; Wang, Y.; Yang, X.-Q.; Wang, C. Solvation Structure Design for Aqueous Zn Metal Batteries. *J. Am. Chem. Soc.* **2020**, *142* (51), 21404–21409.
- (10) Liu, S.; Lei, T.; Song, Q.; Zhu, J.; Zhu, C. High Energy, Long Cycle, and Superior Low Temperature Performance Aqueous Na-Zn Hybrid Batteries Enabled by a Low-Cost and Protective Interphase Film-Forming Electrolyte. *ACS Appl. Mater. Interfaces* **2022**, *14* (9), 11425–11434.
- (11) Pan, W.; Wang, Y.; Zhao, X.; Zhao, Y.; Liu, X.; Xuan, J.; Wang, H.; Leung, D. Y. C. High-Performance Aqueous Na–Zn Hybrid Ion Battery Boosted by “Water-In-Gel” Electrolyte. *Adv. Funct. Mater.* **2021**, *31* (15), No. 2008783.
- (12) Hu, P.; Zhu, T.; Wang, X.; Zhou, X.; Wei, X.; Yao, X.; Luo, W.; Shi, C.; Owusu, K. A.; Zhou, L.; et al. Aqueous Zn//Zn(CF₃SO₃)₂//Na₃V₂(PO₄)₃ batteries with simultaneous Zn²⁺/Na⁺ intercalation/de-intercalation. *Nano Energy* **2019**, *58*, 492–498.
- (13) Li, G.; Yang, Z.; Jiang, Y.; Zhang, W.; Huang, Y. Hybrid aqueous battery based on Na₃V₂(PO₄)₃/C cathode and zinc anode for potential large-scale energy storage. *J. Power Sources* **2016**, *308*, 52–57.
- (14) Wang, L.-P.; Wang, P.-F.; Wang, T.-S.; Yin, Y.-X.; Guo, Y.-G.; Wang, C.-R. Prussian blue nanocubes as cathode materials for aqueous Na-Zn hybrid batteries. *J. Power Sources* **2017**, *355*, 18–22.
- (15) Zhao, S.; Zhang, Y.; Li, J.; Qi, L.; Tang, Y.; Zhu, J.; Zhi, J.; Huang, F. A Heteroanionic Zinc Ion Conductor for Dendrite-Free Zn Metal Anodes. *Adv. Mater.* **2023**, *35* (18), No. 2300195.
- (16) Zhao, Z.; Wang, R.; Peng, C.; Chen, W.; Wu, T.; Hu, B.; Weng, W.; Yao, Y.; Zeng, J.; Chen, Z.; et al. Horizontally arranged zinc platelet electrodeposits modulated by fluorinated covalent organic framework film for high-rate and durable aqueous zinc ion batteries. *Nat. Commun.* **2021**, *12* (1), 6606.
- (17) Lu, X.; Jimenez-Rioboo, R. J.; Leech, D.; Gutierrez, M. C.; Ferrer, M. L.; Del Monte, F. Aqueous-Eutectic-in-Salt Electrolytes for High-Energy-Density Supercapacitors with an Operational Temperature Window of 100 degrees C, from –35 to + 65 degrees C. *ACS Appl. Mater. Interfaces* **2020**, *12* (26), 29181–29193.
- (18) Nian, Q.; Wang, J.; Liu, S.; Sun, T.; Zheng, S.; Zhang, Y.; Tao, Z.; Chen, J. Aqueous Batteries Operated at –50 degrees C. *Angew. Chem., Int. Ed.* **2019**, *58* (47), 16994–16999.
- (19) Cao, L.; Li, D.; Hu, E.; Xu, J.; Deng, T.; Ma, L.; Wang, Y.; Yang, X. Q.; Wang, C. Solvation Structure Design for Aqueous Zn Metal Batteries. *J. Am. Chem. Soc.* **2020**, *142* (51), 21404–21409.
- (20) Lu, X.; Hansen, E. J.; He, G.; Liu, J. Eutectic Electrolytes Chemistry for Rechargeable Zn Batteries. *Small* **2022**, *18* (21), No. 2200550.
- (21) Yu, W.; Liu, Y.; Liu, L.; Yang, X.; Han, Y.; Tan, P. Rechargeable aqueous Zn-LiMn₂O₄ hybrid batteries with high performance and safety for energy storage. *J. Energy Storage* **2022**, *45*, No. 103744.
- (22) Mitha, A.; Yazdi, A. Z.; Ahmed, M.; Chen, P. Surface Adsorption of Polyethylene Glycol to Suppress Dendrite Formation on Zinc Anodes in Rechargeable Aqueous Batteries. *Chem. Electro. Chem.* **2018**, *5* (17), 2409–2418.
- (23) Xing, Z.; Huang, C.; Hu, Z. Advances and strategies in electrolyte regulation for aqueous zinc-based batteries. *Coord. Chem. Rev.* **2022**, *452*, No. 214299.
- (24) Du, W.; Yan, J.; Cao, C.; Li, C. C. Electrocrystallization orientation regulation of zinc metal anodes: strategies and challenges. *Energy Storage Mater.* **2022**, *52*, 329–354.
- (25) Yuan, L.; Hao, J.; Kao, C.-C.; Wu, C.; Liu, H.-K.; Dou, S.-X.; Qiao, S.-Z. Regulation methods for the Zn/electrolyte interphase and the effectiveness evaluation in aqueous Zn-ion batteries. *Energy Environ. Sci.* **2021**, *14* (11), 5669–5689.
- (26) Zhang, R.; Feng, Y.; Ni, Y.; Zhong, B.; Peng, M.; Sun, T.; Chen, S.; Wang, H.; Tao, Z.; Zhang, K. Bifunctional Interphase with Target-Distributed Desolvation Sites and Directionally Depositional Ion Flux for Sustainable Zinc Anode. *Angew. Chem., Int. Ed.* **2023**, *62* (25), No. e202304503.
- (27) Sun, P.; Ma, L.; Zhou, W.; Qiu, M.; Wang, Z.; Chao, D.; Mai, W. Simultaneous Regulation on Solvation Shell and Electrode Interface for Dendrite-Free Zn Ion Batteries Achieved by a Low-Cost Glucose Additive. *Angew. Chem., Int. Ed.* **2021**, *60* (33), 18247–18255.
- (28) Li, W.; Wang, K.; Zhou, M.; Zhan, H.; Cheng, S.; Jiang, K. Advanced Low-Cost, High-Voltage, Long-Life Aqueous Hybrid Sodium/Zinc Batteries Enabled by a Dendrite-Free Zinc Anode and Concentrated Electrolyte. *ACS Appl. Mater. Interfaces* **2018**, *10* (26), 22059–22066.
- (29) Li, C.; Kingsbury, R.; Zhou, L.; Shyamsunder, A.; Persson, K. A.; Nazar, L. F. Tuning the Solvation Structure in Aqueous Zinc Batteries to Maximize Zn-Ion Intercalation and Optimize Dendrite-Free Zinc Plating. *ACS Energy Lett.* **2022**, *7* (1), 533–540.
- (30) Pu, S. D.; Gong, C.; Tang, Y. T.; Ning, Z.; Liu, J.; Zhang, S.; Yuan, Y.; Melvin, D.; Yang, S.; Pi, L.; et al. Achieving Ultra-High Rate Planar and Dendrite-Free Zinc Electroplating for Aqueous Zinc Battery Anodes. *Adv. Mater.* **2022**, *34* (28), No. e2202552.
- (31) Shi, J.; Sun, T.; Bao, J.; Zheng, S.; Du, H.; Li, L.; Yuan, X.; Ma, T.; Tao, Z. Water-in-Deep Eutectic Solvent” Electrolytes for High-Performance Aqueous Zn-Ion Batteries. *Adv. Funct. Mater.* **2021**, *31* (23), No. 2102035.
- (32) Geng, L.; Wang, X.; Han, K.; Hu, P.; Zhou, L.; Zhao, Y.; Luo, W.; Mai, L. Eutectic Electrolytes in Advanced Metal-Ion Batteries. *ACS Energy Lett.* **2022**, *7* (1), 247–260.
- (33) Yang, W.; Du, X.; Zhao, J.; Chen, Z.; Li, J.; Xie, J.; Zhang, Y.; Cui, Z.; Kong, Q.; Zhao, Z.; et al. Hydrated Eutectic Electrolytes with Ligand-Oriented Solvation Shells for Long-Cycling Zinc-Organic Batteries. *Joule* **2020**, *4* (7), 1557–1574.
- (34) Zhang, C.; Zhang, L.; Yu, G. Eutectic Electrolytes as a Promising Platform for Next-Generation Electrochemical Energy Storage. *Acc. Chem. Res.* **2020**, *53* (8), 1648–1659.
- (35) Xu, J.; Ji, X.; Zhang, J.; Yang, C.; Wang, P.; Liu, S.; Ludwig, K.; Chen, F.; Kofinas, P.; Wang, C. Aqueous electrolyte design for super-stable 2.5 V LiMn₂O₄ || Li₄Ti₅O₁₂ pouch cells. *Nat. Energy* **2022**, *7* (2), 186–193.
- (36) Jiang, P.; Chen, L.; Shao, H.; Huang, S.; Wang, Q.; Su, Y.; Yan, X.; Liang, X.; Zhang, J.; Feng, J.; et al. Methylsulfonylmethane-Based Deep Eutectic Solvent as a New Type of Green Electrolyte for a High-Energy-Density Aqueous Lithium-Ion Battery. *ACS Energy Lett.* **2019**, *4* (6), 1419–1426.
- (37) Smith, E. L.; Abbott, A. P.; Ryder, K. S. Deep Eutectic Solvents (DESS) and Their Applications. *Chem. Rev.* **2014**, *114* (21), 11060–11082.
- (38) Han, D.; Sun, T.; Zhang, R.; Zhang, W.; Ma, T.; Du, H.; Wang, Q.; He, D.; Zheng, S.; Tao, Z. Eutectic Electrolytes with Doubly-Bound Water for High-Stability Zinc Anodes. *Adv. Funct. Mater.* **2022**, *32* (52), No. 2209065.
- (39) Zhao, J.; Zhang, J.; Yang, W.; Chen, B.; Zhao, Z.; Qiu, H.; Dong, S.; Zhou, X.; Cui, G.; Chen, L. Water-in-deep eutectic solvent” electrolytes enable zinc metal anodes for rechargeable aqueous batteries. *Nano Energy* **2019**, *57*, 625–634.
- (40) Sun, H.; Ren, P.; Fried, J. R. The COMPASS force field: parameterization and validation for phosphazenes. *Comput. Theor. Polym. Sci.* **1998**, *8* (1–2), 229–246.
- (41) Chen, Q.; Zhuang, W.; Hou, Z.; Jiang, Y.; Wan, J.; Zhang, T.; Zhao, Y.; Huang, L. A Dual-Function Additive to Regulate Nucleation Behavior and Interfacial Chemistry for Ultra-Stable Na Metal Anodes beyond One Year. *Adv. Funct. Mater.* **2023**, *33* (4), No. 2210206.
- (42) Henderson, W. A.; McKenna, F.; Khan, M. A.; Brooks, N. R.; Young, V. G.; Frech, R. Glyme-lithium bis(trifluoromethanesulfonyl)imide and glyme-lithium bis(perfluoroethanesulfonyl)imide phase

behavior and solvate structures. *Chem. Mater.* **2005**, *17* (9), 2284–2289.

(43) Zhang, Y. H.; Chan, C. K. Observations of water monomers in supersaturated NaClO₄, LiClO₄, and Mg(ClO₄)₂ droplets using Raman spectroscopy. *J. Phys. Chem. A* **2003**, *107* (31), 5956–5962.

(44) Auer, B. M.; Skinner, J. L. IR and Raman spectra of liquid water: Theory and interpretation. *J. Chem. Phys.* **2008**, *128* (22), 224511.

(45) Patel, M. B.; Agarwal, A.; Bist, H. D. Single-Crystal Raman Spectra of Magnesium and Zinc Perchlorate Hexahydrates. *J. Raman Spectrosc.* **1983**, *14* (6), 406–440.

(46) Rudolph, W. W.; Fischer, D.; Irmer, G. Hydration and Ion-Pair Formation of NaNO₃(aq): A Vibrational Spectroscopic and Density Functional Theory Study. *Appl. Spectrosc.* **2021**, *75* (4), 395–411.

(47) Legrand, L.; Tranchant, A.; Messina, R.; Romain, F.; Lautie, A. Raman study of aluminum chloride dimethylsulfone solutions. *Inorg. Chem.* **1996**, *35* (5), 1310–1312.

(48) Wan, F.; Zhang, L.; Dai, X.; Wang, X.; Niu, Z.; Chen, J. Aqueous rechargeable zinc/sodium vanadate batteries with enhanced performance from simultaneous insertion of dual carriers. *Nat. Commun.* **2018**, *9* (1), 1656.

(49) Zhang, X.; Li, J.; Liu, D.; Liu, M.; Zhou, T.; Qi, K.; Shi, L.; Zhu, Y.; Qian, Y. Ultra-long-life and highly reversible Zn metal anodes enabled by a desolvation and deamination interface layer. *Energy Environ. Sci.* **2021**, *14* (5), 3120–3129.

(50) Cao, L.; Li, D.; Soto, F. A.; Ponce, V.; Zhang, B.; Ma, L.; Deng, T.; Seminario, J. M.; Hu, E.; Yang, X.-Q.; et al. Highly Reversible Aqueous Zinc Batteries enabled by Zincophilic–Zincophobic Interfacial Layers and Interrupted Hydrogen-Bond Electrolytes. *Angew. Chem. Int. Ed.* **2021**, *60* (34), 18845–18851.

(51) Es-Smairi, A.; Fazouan, N.; Joshi, H.; Atmani, E. H. First-principles calculations to investigate electronic, optical, thermodynamic and thermoelectric properties of new Na₆ZnX₄ (X = O, S, Se) ternary alloys. *J. Phys. Chem. Solids* **2022**, *160*, No. 110305.

(52) Jiang, P.; Shao, H.; Chen, L.; Feng, J.; Liu, Z. Ion-selective copper hexacyanoferrate with an open-framework structure enables high-voltage aqueous mixed-ion batteries. *J. Mater. Chem. A* **2017**, *5* (32), 16740–16747.

(53) Wang, Y.; Wang, Z.; Pang, W. K.; Lie, W.; Yuwono, J. A.; Liang, G.; Liu, S.; Angelo, A. M.; Deng, J.; Fan, Y.; et al. Solvent control of water O-H bonds for highly reversible zinc ion batteries. *Nat. Commun.* **2023**, *14* (1), 2720.

(54) Li, Q.; Yang, C.; Zhang, J.; Ji, X.; Xu, J.; He, X.; Chen, L.; Hou, S.; Uddin, J.; Addison, D.; et al. Controlling Intermolecular Interaction and Interphase Chemistry Enabled Sustainable Water-tolerance LiMn₂O₄||Li₄Ti₅O₁₂ Batteries. *Angew. Chem., Int. Ed.* **2022**, *61* (49), No. e2214126.